Proceedings of the
44th IEEE Conference on Decision and Control, and
the European Control Conference 2005
Seville, Spain, December 12-15, 2005

Timing Feedback Control of a Rhythmic System

Renaud Ronsse, Philippe Lefevre and Rodolphe Sepulchre

Abstract— **This paper addresses the question relative to the role of sensory feedback in rhythmic tasks. We study the properties of a sinusoidally vibrating wedge-billiard as a model for 2-D bounce juggling. If this wedge is actuated with an harmonic sinusoidal input, it has been shown that some periodic orbits are exponentially stable. This paper explores an intuitive method to enlarge the parametric stability region of the simplest of these orbits. Accurate processing of *timing* is proven to be an important key to achieve frequency-locking in rhythmic tasks.**

I. INTRODUCTION

How much sensory information is needed to perform a rhythmic task and how is this information integrated to periodically produce intermittent control actions ? This issue reaches across a number of disciplines and seems relevant not only to animal behavior modeling but also to rhythmic robotics. But it has received limited attention in the control community beyond the pioneering work of Koditschek and coworkers, initially in juggling robotics [1], [2], [3] and more recently in legged robotics [4].

The rhythmic task we consider in this paper is based on a simplified juggling task. The planar wedge-billiard we consider has been previously presented in [5], [6], [7]. This robotic device is viewed as an idealization of a human juggler: the ball in a constant gravitational field undergoes collisions with two edges, acting the juggler arms.

In [6] and [7], we emphasized how a simple sensorless sinusoidal actuation of the edges could achieve exponential stability of periodic orbits which mimics the popular *shower* juggling pattern. This stability result can be interpreted as a 2-D generalization of the celebrated bouncing ball dynamics [8], [9]. The sinusoidal actuation exploits the intermittent nature of control to achieve stability of the impact *times*. The juggled ball velocity is regulated by the decelerating motion (at impact) of the edges. In the present paper, we enhance this stabilizing mechanism based on a simple proportional feedback, the output being an estimate of the timing of the forthcoming impact. The proportional output feedback (FB) loop enlarges the parametric stability region of the feedforward (FF) sinusoidal actuation. The relative timing between the controller and the controlled object, i.e. in this case, the *phase* between the edges and the ball, is therefore proved to be an important information to control the rhythmic task.

This work was supported by the Belgian Program on Interuniversity Attraction Poles initiated by the Belgian Federal Science Policy Office.

R. Ronsse and R. Sepulchre are with the Department of Electrical Engineering and Computer Science (Montefiore Institute), Université de Liège, 4000 Liège, Belgium [R.Ronsse,R.Sepulchre]@ulg.ac.be

P. Lefevre is with the Center for Systems Engineering and Applied Mechanics (CESAME), Université catholique de Louvain, 1348 Louvain-la-Neuve, Belgium lefevre@csam.ucl.ac.be

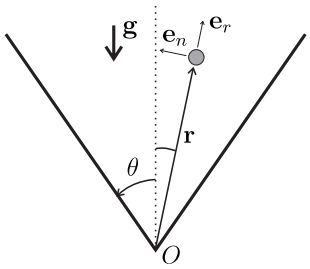

Fig. 1. The wedge-billiard.

The role of sensory feedback in rhythmic tasks remains an outstanding puzzle in animal behavior modeling. While a discrete action such as pointing or grasping can be interpreted as a path planning control problem [10], [11], this is however less evident to understand how sensory feedback is integrated during rhythmic tasks. Recent papers have particularly investigated the differences in motor programming of equivalent rhythmic and discrete tasks [12], [13]. Aiming at focusing on the particular role of sensory feedback in the control loop of rhythmic tasks, we point out the paper of Kuo [14] which disentangles the role of FF and FB paths in a simple rhythmic task. It focuses mainly on the role of the central pattern generator[1] (CPG). In the present paper, we exhibit how steady-state control of a rhythmic task rests in fact on the control of its *phase*.

The paper is organized as follows: in Section II, we review the wedge-billiard model and its steady-state periodic orbits. We summarize also the results on the feedforward stabilization. In Section III, we will show how the role played by the vibration amplitude in the feedforward approach could be reinterpreted as a proportional feedback tuning the vibration *amplitude* as a function of a *phase* prediction. This significantly enlarges the parametric stability region of the feedforward input. This proportional controller achieves stability over a large range of gain, giving therefore the gain stability margin which is illustrated in Section IV. In Section V, we briefly outline the future implementation of this feedback loop in the lab. The paper ends with a conclusion.

II. A SIMPLIFIED JUGGLER

A. Model

The dynamical system studied in this paper is an idealization of a human juggler. We consider a motion restricted to

[1]CPGs are neural circuits that generate periodic motor commands for rhythmic movements.

a plane under a constant gravitational field $\mathbf{g}$ (with $|\mathbf{g}| = g$). The juggled ball undergoes collisions with two edges, which act as the juggler arms (see Fig. 1). In contrast to human juggling, the impacts between the "hands" and the ball are supposed to be instantaneous, hence the name *impact* (or *bounce*) juggling. This paper focuses on patterns involving one ball.

Our model is an actuated version of the model introduced in [15] and was first presented in [5] in order to study feedback stabilization schemes of juggling patterns. The four-dimensional wedge billiard dynamics are studied via the three-dimensional discrete Poincaré map relating the state *from one impact to the next one*, the ball motion between two impacts being parabolic (a ballistic flight in a constant gravitational field $\mathbf{g}$). Let $(\mathbf{e}_r,\mathbf{e}_n)$ be an orthonormal frame attached to the fixed point O with $\mathbf{e}_r$ aligned with the ball position vector $\mathbf{r} = r\mathbf{e}_r$. The ball is assumed to be a unit mass point, let $\mathbf{v} = v_r\mathbf{e}_r + v_n\mathbf{e}_n$ denote its velocity. Therefore the discrete state vector denotes the state of the ball at the impacts. This state being discontinuous at the impacts, we choose the post-impact values to make up the state vector as a convention:

$$\mathbf{x}[k] \equiv \begin{pmatrix} V_r[k] \\ |V_n|[k] \\ R[k] \end{pmatrix} = \begin{pmatrix} V_r^+(t[k]) \\ |V_n^+|(t[k]) \\ R^+(t[k]) \end{pmatrix}$$

where $V_r = \frac{v_r}{\cos\theta}$, $V_n = \frac{v_n}{\sin\theta}$ and $R = \frac{r}{\cos\theta}$ denote the state of the ball and the $\bullet^+$ notations denote the post-impact values, evaluated at impact time $t[k]$. The corresponding pre-impact values are denoted $\bullet^-$. We consider the absolute value of the normal velocity, the wedge-billiard being symmetric with respect to its bisecting line.

The discrete wedge-billiard map is the composition of an impact rule and a parabolic flight map. The impact rule $\mathcal{I}$ adopted is derived from the Newton's impact law: the normal velocity is reversed, proportionally to a *coefficient of restitution* e modeling the energy dissipation at impact ($0 \leq e \leq 1$), while the tangential velocity is conserved. This paper focuses on solutions implying an *actuation* of the edges in order to feed some energy to the ball at each impact. This control input is captured in the impact rule where the normal velocity expression is therefore expressed *relatively* to the edge velocity:

$$V_n[k] - \dot{s}[k] = -e\left(V_n^-(t[k]) - \dot{s}[k]\right)$$

where $\dot{s}[k] = \dot{s}(t[k]) = \frac{\dot{\tilde{s}}(t[k])}{\sin\theta}$ and $\dot{\tilde{s}}(t[k])$ denotes the edge velocity at the impact time $t[k]$. The impact rule $\mathcal{I}$ is then:

$$\begin{aligned} V_r[k] &= V_r^-(t[k]) \\ V_n[k] &= -eV_n^-(t[k]) + (1+e)\dot{s}[k] \end{aligned} \tag{1}$$

Considering the *unactuated* wedge-billiard [15], the flight map is the velocity and position update of the ball integrated through a flight between two impacts. Two different flight maps must be considered whether these impacts occur on the same edge or not. These flight maps have been derived in [5]. The rest of this paper focusing only on solutions, and

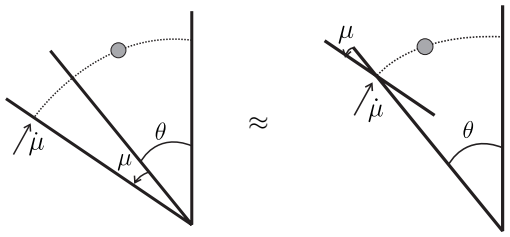

Fig. 2. The controlled rotational wedge (left), and the simplified model when μ is small (right).

stability properties, where the ball hits the edges alternately, the wedge-billiard map is therefore the composition of the impact rule $\mathcal{I}$ (1) and the second flight map. One obtains the discrete billiard map $\mathcal{B}$:

$$\begin{aligned} V_r[k+1] &= |V_n|[k] - V_r[k] - |V_n^-|[k+1] \\ V_n[k+1] &= -e\,|V_n^-|[k+1]\ \mathrm{sign}(V_n[k]) \\ &\quad +(1+e)\dot{s}[k+1] \\ R[k+1] &= R[k] - \frac{1}{2g}(V_r^2[k+1] - V_r^2[k]) \\ &\quad -\frac{\alpha^2}{2g}(|V_n^-|^2[k+1] - V_n^2[k]) \end{aligned} \tag{2}$$

where $|V_n^-|[k+1]$ denotes the absolute value of the ball normal velocity just before impact $[k+1]$:

$$|V_n^-|[k+1] = \sqrt{\left(\tfrac{2V_r[k]+(\alpha^2-1)|V_n|[k]}{1+\alpha^2}\right)^2 + \tfrac{4g}{1+\alpha^2}R[k]} \tag{3}$$

with

$$\alpha = \tan\theta$$

The position update of (2) derives from the *energy* expression:

$$E[k] = \frac{1}{1+\alpha^2}\left(\frac{1}{2}V_r^2[k] + \frac{\alpha^2}{2}V_n^2[k] + gR[k]\right) \tag{4}$$

and the conservation of energy through the flight implies: $E^-[k+1] = E[k]$.

For later reference, one also notes the flight time equation given by:

$$\begin{aligned} \Delta t[k] &\equiv t[k+1] - t[k] \\ &= \frac{1}{g}\left(|V_n^-|[k+1] + \frac{(\alpha^2-1)|V_n|[k] + 2V_r[k]}{1+\alpha^2}\right) \end{aligned} \tag{5}$$

Considering now the rotational actuation, the angle θ of each edge with the vertical is no longer constant, which significantly complicates the derivation of the flight map. To avoid the complication of computing that new flight map, a "small amplitude" assumption is introduced: we neglect the variation of θ in the derivation of the flight map but only take it into account in the derivation of the impact map. As illustrated on Fig. 2, this simplification amounts to assume that the impacts always occur at angle θ but that the angular actuation μ rotates the normal and *tangential* directions of the impacted edge by an angle μ (Fig. 2, right). This simplification neglects the displacement of the impact

$$M(\mu[k])\begin{pmatrix} V_r[k] \\ V_n[k] \end{pmatrix} = \begin{pmatrix} 1 & 0 \\ 0 & -e \end{pmatrix} M(\mu[k]) \begin{pmatrix} V_r^-(t[k]) \\ V_n^-(t[k]) \end{pmatrix} + \begin{pmatrix} 0 \\ \frac{1+e}{\alpha} R[k] \end{pmatrix} \dot{\mu}[k] \tag{6}$$

$$\begin{pmatrix} V_r[k+1] \\ V_n[k+1] \end{pmatrix} = J(\mu[k+1]) \begin{pmatrix} |V_n|[k] - V_r[k] - |V_n^-|[k+1] \\ |V_n^-|[k+1].\,\mathrm{sign}(V_n[k]) \end{pmatrix} + \frac{1+e}{\alpha} \begin{pmatrix} -\alpha \sin\mu[k+1] R[k+1] \\ \cos\mu[k+1] R[k+1] \end{pmatrix} \dot{\mu}[k+1] \tag{7}$$

$$R[k+1] = R[k] + \frac{1}{2g} V_r^2[k] + \frac{\alpha^2}{2g} V_n^2[k] - \frac{1}{2g}(|V_n|[k] - V_r[k] - |V_n^-|[k+1])^2 - \frac{\alpha^2}{2g}|V_n^-|^2[k+1]$$

with

$$J(\mu) = M(-\mu) \begin{pmatrix} 1 & 0 \\ 0 & -e \end{pmatrix} M(\mu) = \begin{pmatrix} \cos^2\mu - e\sin^2\mu & \frac{\alpha(1+e)}{2}\sin 2\mu \\ \frac{1+e}{2\alpha}\sin 2\mu & \sin^2\mu - e\cos^2\mu \end{pmatrix} \tag{8}$$

point and is more likely if $|\mu| \ll \theta$. The final impact rule $\mathcal{I}$ is now given by (6) with $M(\mu)$ denoting the rotation matrix of the edge:

$$M(\mu) = \begin{pmatrix} \cos\mu & \alpha\sin\mu \\ -\frac{\sin\mu}{\alpha} & \cos\mu \end{pmatrix}$$

and $\mu[k] = \mu(t[k])$ ($\dot{\mu}[k] = \dot{\mu}(t[k])$) denoting the edge position (velocity) at impact time $t[k]$.

The presence of $R[k]$ in (6) is due to a second important feature introduced by the rotational actuation: the energy exchange with the edges depends now on the impact position $R[k]$. The map $\tilde{\mathcal{B}}$ of the rotational wedge is given by (7).

B. Steady-state orbits with a harmonic actuation

In [6] and [7], we studied the behavior of the wedge-billiard actuated with a harmonic sinusoidal input:

$$\mu(t) = A\sin(\omega t) - C_{\{r,l\}} \tag{9}$$

where C_r and C_l are constants that are tuned such that $\mu[k] = 0$ for the *steady-state* orbits.

This simple *sensorless* actuation of the wedge-billiard has been proven to be a 2-D generalization of the extensively studied "bouncing ball" system [8], [9]. In fact, the dynamics of the *square* wedge-billiard ($\alpha = 1 \Leftrightarrow \theta = 45°$: the edges form a right angle) decouple into the dynamics of two independent 1-D bouncing balls, one along each edge. For this simple case, the steady-state periodic orbits are shown in Tab. I. Indeed, a steady-state regime is characterized by two frequency-locking relations between the ball an the wedge:

$$(t[k+2] - t[k])^\star \equiv \Delta t^{r\star} + \Delta t^{l\star} = n\frac{2\pi}{\omega} \tag{10}$$

$$(t[k+1] - t[k])^\star \equiv \Delta t^{r\star} = (2m-1)\frac{\pi}{\omega} \tag{11}$$

where $(\bullet)^\star$ denotes the steady-state solutions. These relations rest on the trivial assumption $m \leq n$, m and n being positive integers. Equation (10) expresses that the ball period is a multiple of the edge vibration period: this is the frequency-locking relation of each dynamics. Equation (11) expresses that the phase difference between two successive impacts must be equal to an odd multiple of the vibration half-frequency. As a convention, m will be associated with the flight time between the right edge and the left edge: $\Delta t^{r\star} = (2m-1)\frac{\pi}{\omega}$, while the flight time between the left edge and the right edge will be $\Delta t^{l\star} = (2n-2m+1)\frac{\pi}{\omega}$ in the steady-state regime. A well sustained steady-state shower pattern will be characterized exactly by the same ratios, n denoting also the number of juggled balls. It is interesting to point out how the symmetry of the square wedge-billiard captures the symmetry of the juggler behavior.

The *general* wegde-billiard ($\alpha \neq 1$) possesses topologically equivalent periodic orbits. Note however that the period-two orbits ($(x:y) \neq (1:1)$) are no longer characterized by exact ratios between flight times: indeed there is a symmetry breaking in the energy of the ball within both parabolas.

The rest of this paper will be devoted to the analysis of the period-one orbits ($n = 2m-1$). In this case, a periodic orbit corresponds to a fixed point of the Poincaré map (7). According to [6] and [7], this fixed point is:

$$V_r{}^\star = 0 \tag{12}$$

$$|V_n{}^\star| = \frac{1+\alpha^2}{\alpha^2}\frac{(2m-1)\pi g}{2\omega} \tag{13}$$

$$R^\star = \frac{1+\alpha^2}{4\alpha^2}\left(\frac{(2m-1)\pi}{\omega}\right)^2 g \tag{14}$$

Note that

$$E^\star = \frac{3+\alpha^2}{8\alpha^2}\left(\frac{(2m-1)\pi g}{\omega}\right)^2 \tag{15}$$

is the energy of these orbits.

The sinusoidal actuation adds a fourth state variable, i.e. the *phase* of the edges vibration. Its iteration equation is

TABLE I

PERIODIC ORBITS FOR THE SQUARE WEDGE-BILLIARD. $(x:y)$ DENOTES THE RATIO BETWEEN BOTH FLIGHT TIMES WHERE x (y) IS ASSOCIATED WITH THE FLIGHT FROM LEFT TO RIGHT (FROM RIGHT TO LEFT).

	m=1	m=2	m=3	m=4	…
n=1		X	X	X	
n=2			X	X	
n=3				X	…
n=4					
⋮			⋮		

$$\begin{pmatrix} \frac{\omega}{g}\delta V_r[k+1] \\ \frac{\omega}{g}\delta|V_n|[k+1] \\ \frac{\omega^2}{\pi g}\delta R[k+1] \\ \omega\delta t[k+1] \end{pmatrix} = \tilde{\mathcal{M}} \begin{pmatrix} \frac{\omega}{g}\delta V_r[k] \\ \frac{\omega}{g}\delta|V_n|[k] \\ \frac{\omega^2}{\pi g}\delta R[k] \\ \omega\delta t[k] \end{pmatrix} \tag{16}$$

with

$$\tilde{\mathcal{M}} = \begin{pmatrix} \frac{1-4\alpha^2-\alpha^4}{(1+\alpha^2)^2} - 2\mu_{11} & \frac{4\alpha^2}{(1+\alpha^2)^2} - (\alpha^2-1)\mu_{11} & -\frac{4\alpha^2}{(2m-1)(1+\alpha^2)^2} - \frac{2}{(2m-1)}\mu_{11} & -\frac{1-e}{1+e}2(1+\alpha^2) \\ \frac{2e(\alpha^2-1)}{(1+\alpha^2)^2} + (2m-1)\mu_{21} & \frac{e(\alpha^2-1)^2}{(1+\alpha^2)^2} + \mu_{22} & \frac{4e\alpha^2}{(2m-1)(1+\alpha^2)^2} + \mu_{21} & -\frac{(1-e)(1+\alpha^2)(2m-1)^2\Gamma'}{4\alpha^3} \\ \frac{(2m-1)(1-\alpha^2)}{1+\alpha^2} & \frac{2(2m-1)\alpha^2}{1+\alpha^2} & \frac{1-\alpha^2}{1+\alpha^2} & 0 \\ \frac{4\alpha^2}{(1+\alpha^2)^2} & \frac{2\alpha^2(\alpha^2-1)}{(1+\alpha^2)^2} & \frac{4\alpha^2}{(2m-1)(1+\alpha^2)^2} & 1 \end{pmatrix} \tag{17}$$

$$\mu_{11} = \frac{1-e}{1+e}\frac{4\alpha^2}{1+\alpha^2} \qquad \mu_{22} = (1-e)\left(\frac{(1-\alpha^2)(2m-1)^2\Gamma'}{2\alpha(1+\alpha^2)} + \frac{4\alpha^2}{1+\alpha^2}\right)$$

$$\mu_{21} = (1-e)\left(\frac{-(2m-1)\Gamma'}{\alpha(1+\alpha^2)} + \frac{2(1-\alpha^2)}{(2m-1)(1+\alpha^2)}\right) \qquad \Gamma' = \sqrt{\left(\left(\frac{1+e}{1-e}\right)A\pi^2\right)^2 - \left(\frac{2\pi\alpha}{2m-1}\right)^2} \tag{18}$$

simply given by the the flight time equation (5) while its steady-state value is:

$$\phi^\star = \arccos\left(\frac{1-e}{1+e}\frac{2\alpha}{A}\frac{1}{(2m-1)\pi}\right)[-\pi] \tag{19}$$

The $[-\pi]$ applying to the left arm. The steady-state phase corresponds to the point where the edge compensates exactly for the energy dissipated by the impact. The actuation offsets are therefore:

$$C_r = -A\sin\phi^\star \tag{20}$$

$$C_l = A\sin\phi^\star \tag{21}$$

The *stability* is studied via the linearized Poincaré map of $\tilde{\mathcal{B}}$ (7) and of the flight time (5) around the period-one solution just derived. We find the Jacobian matrix (16). Note that the determinant of $\tilde{\mathcal{M}}$ is equal to

$$|\tilde{\mathcal{M}}| = \frac{e\left((1-e)(3\alpha^2-1)+2(1+\alpha^2)\right)}{(1+e)(1+\alpha^2)} \tag{22}$$

which is equal to 1 in the elastic case ($e = 1$), $\forall\alpha$. This illustrates that the sinusoidal input does not achieve exponential stability of the period-one orbit in the *elastic* wedge, because all the eigenvalues of this matrix cannot be < 1 in that case.

The eigenvalues of (16) were numerically computed for several values of e and α. Fig. 3 depicts the stability region for the first two period-one orbits ($n = 1$, $m = 1$ (a) and $n = 3$, $m = 2$ (b)). The superposed curves stand for different values of e.

A decreasing coefficient of restitution reduces the parametric stability region and shifts it in a zone corresponding to smaller angles between the edges. We can see that even for $e = 0$, the first period-one orbit is still theoretically stabilizable with a sinusoidal vibration of the edges if the impacts occur with $\theta \in [15°, 40°]$.

A sinusoidal actuation of the edges therefore stabilizes period-one orbits, for any coefficient of restitution $e < 1$ and for a broad domain of wedge geometry. For $\theta > 45°$ this exponential stability is in sharp contrast with the instability of the same periodic orbit in the fixed elastic wedge [15].

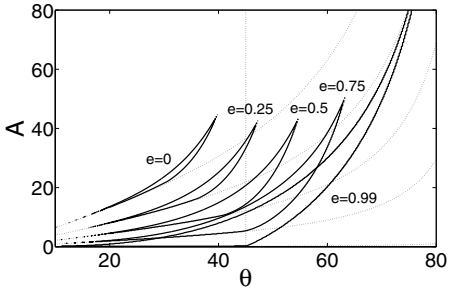

(a) $n = 1$, $m = 1$

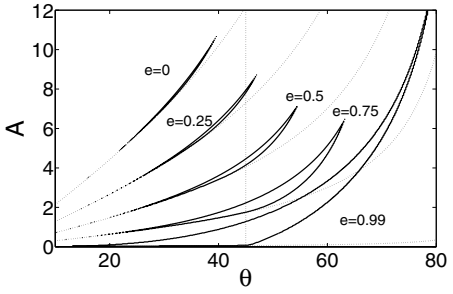

(b) $n = 3$, $m = 2$

Fig. 3. Parametric stability region of two period-one orbits in the general wedge (solid lines). The dotted lines denote the physical minimum value for the amplitude A (the arccos argument in (19) must be ≤ 1).

This result is particularly interesting because the sinusoidal "control" uses no feedback measurement ! The interested reader can find some movies illustrating this *sensorless* stabilization of periodic orbits on `www.montefiore.ulg.ac.be/~ronsse/`.

III. TIMING FEEDBACK

The sinusoidal input $\mu(t) = A\left(\sin(\omega t) \pm \sin(\phi^\star)\right)$ introduced in Section II *isolates* one of the period-one orbits

$$\tilde{\mathcal{M}} = \begin{pmatrix} \frac{1-4\alpha^2-\alpha^4}{(1+\alpha^2)^2} - 2\mu_{11} & \frac{4\alpha^2}{(1+\alpha^2)^2} - (\alpha^2-1)\mu_{11} & -\frac{4\alpha^2}{(2m-1)(1+\alpha^2)^2} - \frac{2}{(2m-1)}\mu_{11} & -\frac{1-e}{1+e}2(1+\alpha^2) \\ \frac{2e(\alpha^2-1)}{(1+\alpha^2)^2} + (1-e)\frac{2(1-\alpha^2)}{1+\alpha^2} & \frac{e(\alpha^2-1)^2}{(1+\alpha^2)^2} + (1-e)\frac{4\alpha^2}{1+\alpha^2} & \frac{4e\alpha^2}{(2m-1)(1+\alpha^2)^2} + (1-e)\frac{2(1-\alpha^2)}{(2m-1)(1+\alpha^2)} & 0 \\ \frac{(2m-1)(1-\alpha^2)}{1+\alpha^2} & \frac{2(2m-1)\alpha^2}{1+\alpha^2} & \frac{1-\alpha^2}{1+\alpha^2} & 0 \\ \frac{4\alpha^2}{(1+\alpha^2)^2} & \frac{2\alpha^2(\alpha^2-1)}{(1+\alpha^2)^2} & \frac{4\alpha^2}{(2m-1)(1+\alpha^2)^2} & 1 \end{pmatrix}$$
$$- \underbrace{\begin{pmatrix} 0 \\ (1-e)\frac{(1+\alpha^2)(2m-1)\pi}{2\alpha^2} \\ 0 \\ 0 \end{pmatrix}}_{\mathbf{B}} \underbrace{\begin{pmatrix} \frac{4\alpha^2}{(1+\alpha^2)^2} & \frac{2\alpha^2(\alpha^2-1)}{(1+\alpha^2)^2} & \frac{4\alpha^2}{(2m-1)(1+\alpha^2)^2} & 1 \end{pmatrix}}_{\mathbf{C}} \frac{2m-1}{2\pi\alpha}\Gamma' \tag{23}$$

existing in the unactuated elastic wedge-billiard.

Existence of a period-one orbit in the non-elastic model imposes a minimal amplitude A indicated by the dotted lines in Fig. 3.

Stability of the period-one orbit extends across the amplitude range over which the matrix $\tilde{\mathcal{M}}$ in (17) has all its eigenvalues within the unit circle. The dependence of $\tilde{\mathcal{M}}$ on the amplitude A is emphasized in (23) since only the parameter Γ' depends on A, see (18). For a given coefficient of restitution e, the parametric stability region in Fig. 3(a) is bounded from above by the stability requirement and from below by the steady-state existence requirement.

We will propose a simple feedback strategy to enlarge the parametric stability region. The control input we introduce is a simple gain in the vibration *amplitude*. The new vibration law is then:

$$\mu(t) = A\left(\sin(\omega t) \pm \sin(\phi^\star)\right)\left(\underbrace{1}_{FF} + \underbrace{\delta u[k]}_{FB}\right) \tag{24}$$

where $\delta u[k]$ denotes the control input. This control input both preserves the same isolated steady-state fixed point, and does not change the periodicity of the sinusoidal vibration.

Restricting to first order terms $\mathcal{O}(\delta)$, this control input affects only the normal velocity update. The linearized update equations become:

$$\begin{pmatrix} \frac{\omega}{g}\delta V_r[k+1] \\ \frac{\omega}{g}\delta|V_n|[k+1] \\ \frac{\omega^2}{\pi g}\delta R[k+1] \\ \omega\delta t[k+1] \end{pmatrix} = \tilde{\mathcal{M}} \begin{pmatrix} \frac{\omega}{g}\delta V_r[k] \\ \frac{\omega}{g}\delta|V_n|[k] \\ \frac{\omega^2}{\pi g}\delta R[k] \\ \omega\delta t[k] \end{pmatrix} + \mathbf{B}\,\delta u[k] \tag{25}$$

where $\mathbf{B}$ has already been defined in (23).

Defining now a proportional output feedback as:

$$\delta u[k] = k_y \delta y[k] \tag{26}$$
$$= k_y \mathbf{C} \begin{pmatrix} \frac{\omega}{g}\delta V_r[k] \\ \frac{\omega}{g}\delta|V_n|[k] \\ \frac{\omega^2}{\pi g}\delta R[k] \\ \omega\delta t[k] \end{pmatrix} \tag{27}$$

We obtain the following closed-loop iteration map:

$$\begin{pmatrix} \frac{\omega}{g}\delta V_r[k+1] \\ \frac{\omega}{g}\delta|V_n|[k+1] \\ \frac{\omega^2}{\pi g}\delta R[k+1] \\ \omega\delta t[k+1] \end{pmatrix} = \left(\tilde{\mathcal{M}} + k_y \mathbf{B}\mathbf{C}\right) \begin{pmatrix} \frac{\omega}{g}\delta V_r[k] \\ \frac{\omega}{g}\delta|V_n|[k] \\ \frac{\omega^2}{\pi g}\delta R[k] \\ \omega\delta t[k] \end{pmatrix} \tag{28}$$

Observing the similarity between (23) and (28), we conclude that the pole locus achieved with a variation of the gain k_y in the closed-loop map is exactly the same as the one corresponding to a variation of Γ' (i.e. a variation of the amplitude A) for the pure feedforward sinusoidal actuation (23). This means that the closed-loop analysis of the feedback control (24) and (26) proceeds from the open-loop analysis, but that the steady-state requirement (on A) has been decoupled from the stability requirement (on k_y).

A closer look at $\tilde{\mathcal{M}}$ (23) reveals that the matrix we have called $\mathbf{C}$ is exactly equal to the fourth row of $\tilde{\mathcal{M}}$. The output signal just defined can then be physically interpreted as a *prediction* of the next impact *phase*:

$$\delta u[k] = k_y \omega \delta t[k+1] \tag{29}$$

The feedback mechanism consists therefore in tuning the vibration amplitude according to this phase prediction.

IV. CLOSED-LOOP GAIN MARGIN

This section aims at quantifying the gain margin of the closed-loop system just derived.

Let's assume that the amplitude A is now fixed. We choose to fix A at its minimal value, i.e. $A = \frac{1-e}{1+e}\frac{2\alpha}{(2m-1)\pi}$. This choice would for instance result from minimum control consideration. For this particular value of A, we have $\Gamma' = 0$.

Fig. 4 depicts the parametric stability region of the first period-one orbit ($n = m = 1$) of the closed-loop system, for $e = 0.5$. This stability region has exactly the same shape as the one obtained with a variation of A, their poles loci being identical. However this region has increased compared to the one in Fig. 3(a), simply because there is no steady-state requirement on k_y. We can see for example that it is now possible to stabilize the period-one orbit with a wedge angle θ close to 0, whereas the open-loop parametric stability region shrank around $\theta = 20^\circ$ for $e = 0.5$.

For any value of the vibration amplitude

$$A > \frac{1-e}{1+e}\frac{2\alpha}{(2m-1)\pi}$$

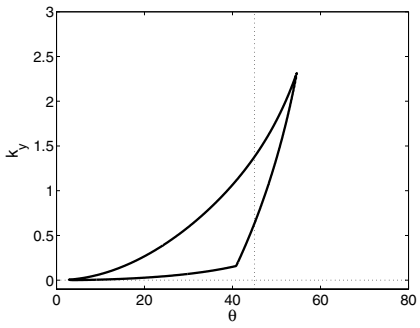

Fig. 4. Parametric stability region of the closed-loop wedge-billiard. $\Gamma' = 0$, $e = 0.5$.

we will obtain the same figure as Fig. 4, with a shift of $\frac{-(2m-1)}{2\pi\alpha}\Gamma'$ downward. The proportional control stabilizes the period-one orbits over a broad range of parameters: $0 \leq \theta_m \leq \theta < \theta_M$ and $\forall A \geq \frac{1-e}{1+e}\frac{2\alpha}{(2m-1)\pi}$. For $e = 0.5$, θ_M is about 54° while θ_m tends to 0°. In this case, θ_M has not changed from the open-loop limit (see the corresponding curve on Fig. 3(a)) while θ_m was only about 20° in that case. Proportional output feedback has therefore significantly enlarged the left-hand side of the parametric stability region.

V. DISCUSSION

The parametric stability region depicted in Fig. 4 is in accordance with the angular region over which human subjects are able to juggle the period-one orbit in a wedge-billiard. We refer the reader to [16] for preliminary results about human strategies in the wedge-billiard. This supports the hypothesis that the simplest feedback loop implemented by human subjects in this task is based on a control of the impact times.

For instance, the control law (24) can be interpreted as an open-loop control between two successive impacts. In the context of the present paper, the *shape* of this control input does not vary over successive impacts (sinusoidal input). Only its *amplitude* is varied based on some feedback information. In current work, we aim at generalizing this idea, while using minimal feedback information for the input shaping.

VI. CONCLUSION

With a model of a simplified juggling task, we showed how to control a particular rhythmic task with a feedforward harmonic input. To increase the parametric stability region, we designed a simple feedback law, based on an prediction of the *phase* between the juggler and the juggled object. This supports the hypothesis that an accurate processing of timing is required to control a rhythmic task.

Section II presented our planar juggler model, called the wedge-billiard. A harmonic sinusoidal vibration of the edges is integrated into this model. This pure feedforward input stabilizes the simplest periodic orbits of the wedge-billiard over a large range of impact angle and vibration amplitude. We designed an output feedback controller in Section III to increase this stability region. This controller predicts the next impact phase to tune the vibration amplitude. In Section IV, the stability region of the controller gain has been illustrated. This gives the margin over which the timing controller achieves stability of the period-one orbit. Future work and implementation issues were outlined in Section V.

REFERENCES

[1] M. Buehler, D. Koditschek, and P. Kindlmann, "A one degree of freedom juggler in a two degree of freedom environment," in *IEEE/RSJ Conf. intelligent Systems and Robots*, Tokyo, Japan, 1988, pp. pp. 91–97.

[2] ——, "A family of robot control strategies for intermittent dynamical environments," *IEEE Control Systems Magazine*, vol. 10, no. 2, pp. pp. 16–22, 1990.

[3] ——, "Planning and control of robotic juggling and catching tasks," *International Journal of Robotics Research*, vol. 13, no. 2, pp. 101–118, 1994.

[4] U. Saranli, M. Buehler, and D. Koditschek, "Rhex - a simple and highly mobile hexapod robot," *International Journal of Robotics Research*, vol. 20, no. 7, pp. 616–631, 2001.

[5] R. Sepulchre and M. Gerard, "Stabilization of periodic orbits in a wedge billiard," in *42nd IEEE Conference on Decision and Control*, Hawaii, 2003.

[6] R. Ronsse, P. Lefevre, and R. Sepulchre, "Open-loop stabilization of 2d impact juggling," in *IFAC NOLCOS*, Stuttgart, Germany, 2004, pp. 1157–1162.

[7] ——, "Sensorless stabilization of bounce juggling," *IEEE Transactions on Robotics*, (accepted).

[8] P. J. Holmes, "The dynamics of repeated impacts with a sinusoidally vibrating table," *J. Sound Vibration*, vol. 84, no. 2, pp. 173–189, 1982.

[9] J. Guckenheimer and P. J. Holmes, *Nonlinear oscillations, dynamical systems and bifurcations of vector fields*. New York: Springer-Verlag, 1986.

[10] J. A. Saunders and D. C. Knill, "Visual feedback control of hand movements," *J Neurosci*, vol. 24, no. 13, pp. 3223–34, 2004.

[11] S. H. Scott, "Optimal feedback control and the neural basis of volitional motor control," *Nat Rev Neurosci*, vol. 5, no. 7, pp. 532–46, 2004.

[12] P. A. Lewis and R. C. Miall, "Distinct systems for automatic and cognitively controlled time measurement: evidence from neuroimaging," *Curr Opin Neurobiol*, vol. 13, no. 2, pp. 250–5, 2003.

[13] S. Schaal, D. Sternad, R. Osu, and M. Kawato, "Rhythmic arm movement is not discrete," *Nat Neurosci*, vol. 7, no. 10, pp. 1136–43, 2004.

[14] A. D. Kuo, "The relative roles of feedforward and feedback in the control of rhythmic movements," *Motor Control*, vol. 6, no. 2, pp. 129–45, 2002.

[15] H. E. Lehtihet and B. N. Miller, "Numerical study of a billiard in a gravitational field," *Phys. D*, vol. 21, no. 1, pp. 93–104, 1986.

[16] R. Ronsse, P. Lefevre, and R. Sepulchre, "Eye-hand coordination in a bimanual bounce juggling task," in *Society for Neuroscience 34th Annual Meeting*, San Diego, CA, 2004.